Polish J. Chem., **78**, 1925–1934 (2004)

Photoresponse of Undoped and W-Doped TiO_2

by M. Radecka, P. Sobaś, A. Trenczek and M. Rękas*

AGH University of Science and Technology, Faculty of Materials Science and Ceramics, al. Mickiewicza 30, 30-059 Kraków, Poland

(Received March 2nd, 2004; revised manuscript May 13th, 2004)

Undoped and W-doped polycrystalline TiO_2 were investigated. The kinetics of recombination processes has been studied. The flat band potential of TiO_2 was determined (–0.11 V in respect to saturated calomel electrode, at pH = 7.8). Basing on the photocurrent experiments, the effect of W concentration on solar energy conversion efficiency was discussed. It was found, that addition of W leads to an increase of solar-to-hydrogen energy efficiency. The maximum energy conversion efficiency has been observed for voltage bias *ca* 0.65 V. The highest energy conversion efficiency has been observed for TiO_2 doped with 0.1 at % W.

Key words: titanium oxide, photoanode, solar energy conversion, photoelectrochemistry

Fujishima and Honda [1] have first shown that light absorbed at a semiconductor-electrolyte interface could lead to decomposition of water into hydrogen and oxygen with little or no added electrical energy. During the last three decades much interest has been devoted to TiO_2 as a photoelectrode material suitable for the production of hydrogen. Studies have been performed on single crystals [1–4] and on polycrystalline material either as a sintered specimen [5–8] or as thin films [9–13]. The main disadvantage of application of TiO_2 as photoanode is the low efficiency of the solar energy conversion into chemical energy of hydrogen. This is related to poor absorption of sunlight, due to a wide energy gap of TiO_2 (*ca* 3 eV) and energy losses in recombination processes of the photoelectron-photohole pairs and ohmic resistivity of the electrode [8]. Several techniques for improving the photo-response of TiO_2, which have led to higher solar energy conversion efficiency, have been proposed so far [14]. The most promising among them seems to be TiO_2 doping by foreign ions. The primary purpose of doping is to increase the electrical conductivity of the semiconductor. The largest conductivity increases are observed for incorporation of W^{6+}, Ta^{5+} and Nb^{5+} into TiO_2 crystal lattice [15]. Optimum doping level for photocurrent quantum efficiency appears to be *ca* 0.1 wt % [16,17]. Tungsten doping has been rarely used [18].

The influences of tungsten concentration in TiO_2 on the performance photo-anode is discussed.

*Author for correspondence; E-mail: rekas@uci.agh.edu.pl

EXPERIMENTAL

Sample preparation. Materials were prepared by thermal decomposition of oxide precursors. Titanium tetraisopropoxide, $Ti[OCH(CH_3)_2]_4$, (Aldrich 97%) and tungsten acid, H_2WO_4, (Aldrich 99.9%) were used as starting materials. Undoped TiO_2 powder was prepared by the hydrolysis of tetraisopropoxide aqueous solution in the presence of H_2O_2 and subsequent evaporation of the precipitate. Powder of tungsten acid was dissolved at 333 K in 30% wt aqueous solution of hydrogen peroxide, H_2O_2, (Aldrich, special purity). The resulting solution was transparent, slightly yellow colored with pH about 1. According to Gennari and Pasquievich [19] the tungsten ions, W^{6+}, are present in this solution as complex ions with $[O_2]^{2-}$ ions and H_2O_2 molecules, $[W_2O_3(O_2)_4(H_2O_2)]^{2-}$. The appropriated mixtures of both powders were obtained by dropping a suitable amount of tetraisopropoxide into stirred tungsten acid solution at temperature close to 273 K. After the evaporation of solvents, obtained powders were dried in air, grinded in agate mortar and then calcined at 673 K during 1 hr (the conditions of calcination were established following the results of TG-DTA measurements). Pellets were formed by uniaxial pressing followed by isostatic pressing and sintering at 1323 K during 2.5 hrs.

Photoelectrochemical cells (PEC). The pellets were placed in a special glass sample holder, which does not allow a contact between the back-side of the photoelectrode and any liquid electrolyte. The surface of the semiconductor electrode, exposed to the electrolyte, was circular with a surface area of *ca* 1 cm^2. Fig. 1 illustrates schematically the PEC used in our experiments.

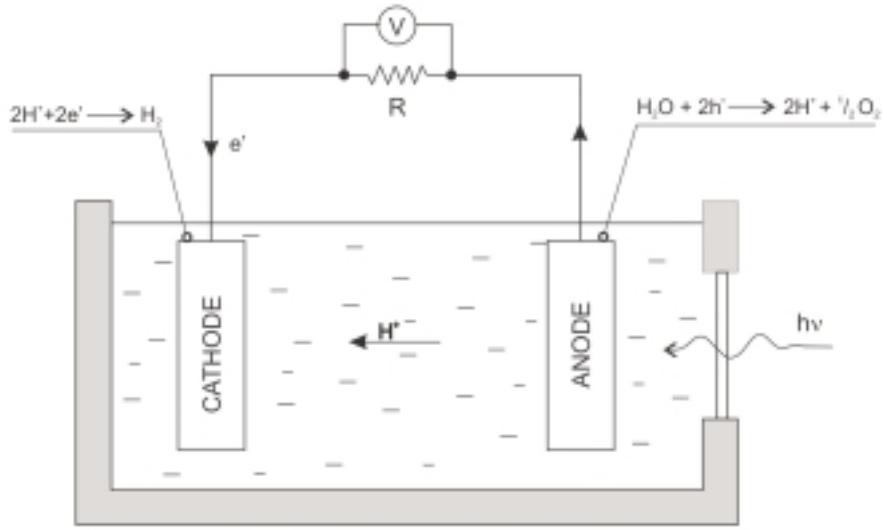

Figure 1. Photo-electrochemical cell, PEC.

A mixture of the universal Britton-Robinson buffer solutions pH = 7.8 with 0.1 M KCl was used as an electrolyte for the electrochemical studies. Such solution with at least of 0.1 M ionic strength exhibits a low electrical resistivity and the Helmholtz layer shows enough high capacitance, which can be negligible in the overall capacitance of the equivalent circuit (the capacitors are connected in series). Pt gauze was used as a cathode.

Photocurrent studies. The photoelectrochemical experiments were carried out using a 450W Xenon lamp as a solar simulated source. The optical system consists of light-source, grating monochromator (Triax 180 Jobin Yvon), optical fibre 1000 μm and photoelectrochemical cell made from plexiglass equipped with quartz window. The cell consisted of an appropriate holder for W-doped TiO_2 photo-electrode, a platinum-black counter electrode, a reference saturated calomel electrode, SCE. The absolute intensity

of the incident light from the monochromator was measured by microcalorimetry (DSC2010 TA Instruments) as described elsewhere [20]. The photo-electrode was placed close to the window of the cell (distance 3–4 mm) to minimize the error, due to the absorption of the light by the solution. The reflection and the absorption of light by window of optical compartment cell were taken into account during the measurement of light intensity.

Photocurrents were measured with a Keithley 6517A electrometer. Bias voltages were supplied from a Hewlett-Packard 34401A power supply. All data acquisition was controlled by PC computer. The photocurrent – time characteristics under constant electrode polarization were obtained with hand – chopped light. The detailed description of measurements is given elsewhere [21].

RESULTS AND DISCUSSION

Figs 2 and 3 show kinetics of photocurrent changes corresponding to successive sudden light switch on and off of the undoped TiO_2 induced by white and monochromatic light, respectively. The characteristic maxima for light on are well shown in the figures and may be described in terms of the two competitive processes: generation of pair electron-hole and their recombination [22,23]. The process of recombination is controlled by the following kinetic equation:

$$D = \exp\left(-\frac{t}{\tau}\right) \qquad (1) \qquad \text{where: D is defined as:} \qquad D = \frac{I(t) - I(f)}{I(i) - I(f)} \qquad (2)$$

t denotes time, τ is parameter defined as transient time constant, I is the photoanode current, the subscripts i and f are related to the initial and final steady states. The transient time may be treated as a lifetime of the photo-excited electron-electron hole pairs [22,23]. The determined average transient time constant from the (1) is *ca* 31.6 s. This is slightly higher than that of TiO_2 thin film sample (27.5 s) [21].

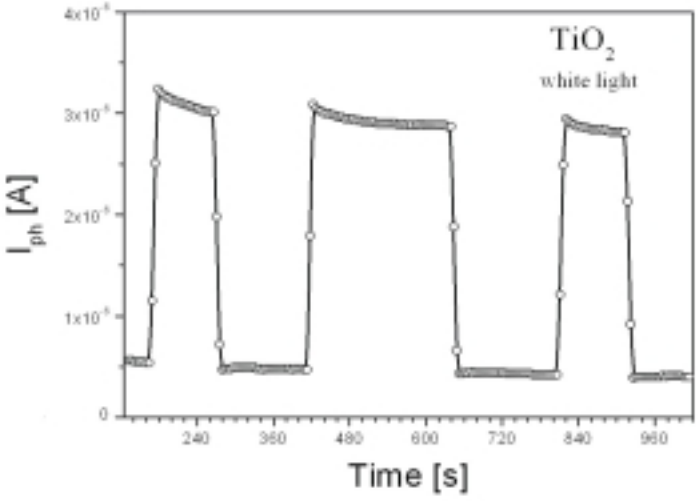

Figure 2. Kinetics of photocurrent of undoped TiO_2, induced by white light.

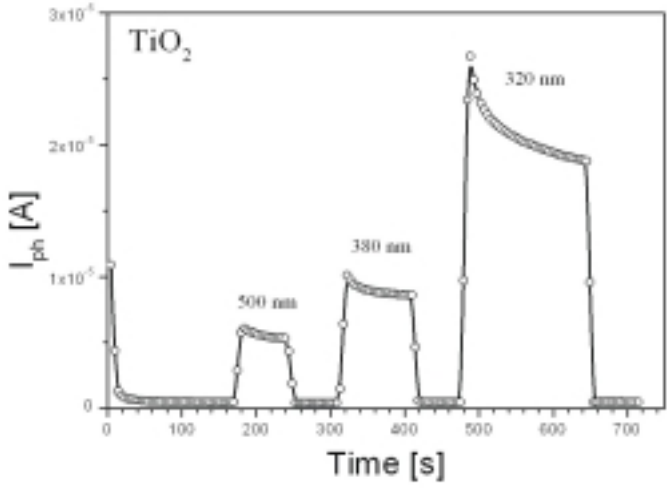

Figure 3. Kinetics of photocurrent of undoped TiO_2, induced by monochromatic light: 320 nm, 380 nm and 500 nm.

Fig. 4 shows log D *vs* time for undoped TiO_2 for monochromatic light corresponding to wavelengths 320 nm, 380 nm and 500 nm. The experimental points may be represented by two straight-line dependencies. At the initial stage slopes of the straight lines assume lower values than that corresponding to the final stages. The observed break of the slopes in Fig. 4 may result from existence more than one different mechanisms of recombination. The determined transient time constant decreases with wavelength of the light. This fact indicates on crucial role of kinetic energies of the photoelectron-photohole pairs on their recombination processes.

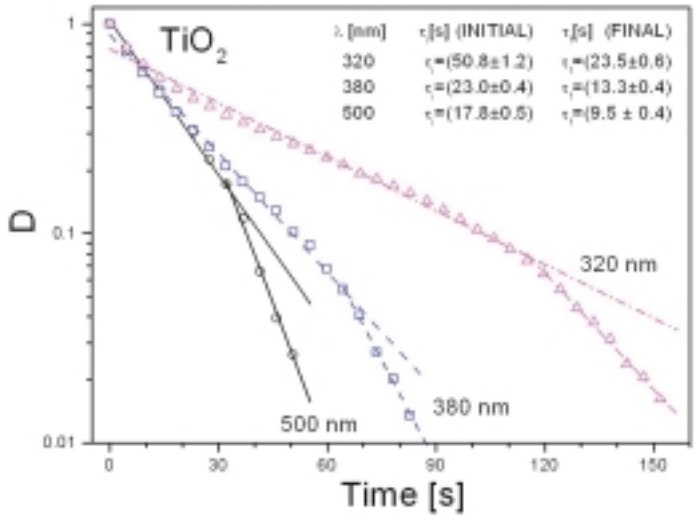

Figure 4. Normalized photocurrent, D, *vs* time dependence induced by monochromatic light (320 nm, 380 nm and 500 nm) of undoped TiO_2.

Current-voltage characteristics at dark and for an illuminated by white light TiO_2 electrode are presented in Fig. 5. Current recorded at dark assumes negligible low values at positive potentials related to a saturated calomel electrode, SCE, below 1.23 V. Then, abrupt increase is observed. This abrupt increase well corresponds to theoretical potential of water decomposition (1.229 V [24]). Photocurrent begins to flow at *ca* –0.06 V, reaches nearly saturation at potential *ca* 1.2 V.

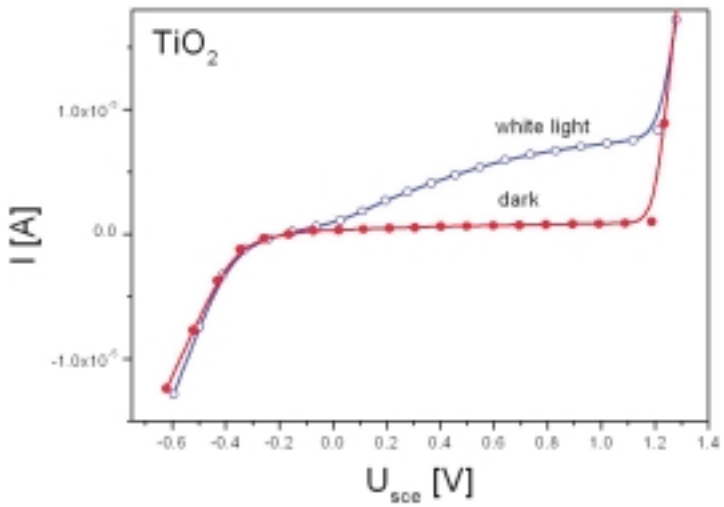

Figure 5. Current-voltage characteristics for undoped TiO_2 monitored in dark and after illumination by white light.

Photocurrent *versus* wavelength of undoped TiO_2 illustrates Fig. 6. The abrupt change of photocurrent with λ within 300 nm–400 nm corresponds to the fundamental light absorption edge, which assumes value about 410 nm in TiO_2 [25]. Then, photocurrent increases with λ, reaching local maximum at 580 nm. The observed photocurrent within forbidden energy region may result from either surface states or subband gap transition [26,27]. Current densities, J_{ph}, corresponding to dark and monochromatic lights are presented in Fig. 7 as a function of U *vs* SCE. Such dependencies are enabling to determine the flat band potential using the following relationship [28]:

$$U - U_{fb} = \left(\frac{N_D}{2e\varepsilon\varepsilon_o}\right)\left(\frac{\Delta J}{\alpha J_R}\right)^2 \tag{3}$$

where U_{fb} – flat band potential, N_D – concentration of donors, e – elementary charge ($1.602 \cdot 10^{-19}$ C), ε – static dielectric constant of the semiconductor, ε_o – permittivity of free space ($8.86 \cdot 10^{-14}$ F/cm), α – light absorption coefficient, W_R – intensity of the light flux entering the semiconductor and:

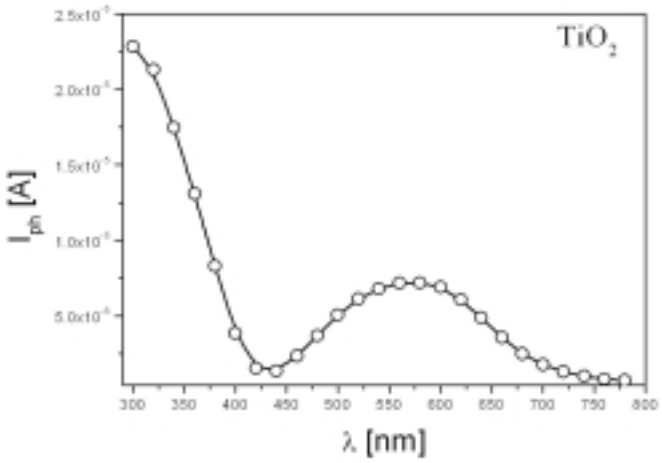

Figure 6. Photocurrent *vs* wavelength for undoped TiO_2.

$$\Delta J = J_{light} - J_{dark} \tag{4}$$

Fig. 8 illustrates the dependencies of $(\Delta J)^2$ as a function of the electrode potential corresponding to photon energies higher (λ = 300 nm, 350 nm, 380 nm – left axis) and lower (λ = 550 nm, 600 nm – right axis) than energy gap (λ_{Eg} = 415 nm). As can be seen, the experimental data fulfill well the theoretical relationship (3). However, the determined U_{fb} parameter from (3) assumes two different values. U_{fb} determined for the energy of incident photons higher than E_g is equal to $-(0.11 \pm 0.01)$ V in respect to SCE, whereas U_{fb} determined for the wavelength 550 nm and 600 nm (*i.e.* photon energies within energy gap of TiO_2) assumes value about –0.34 V. This later U_{fb} cannot be treated as a real flat band potential.

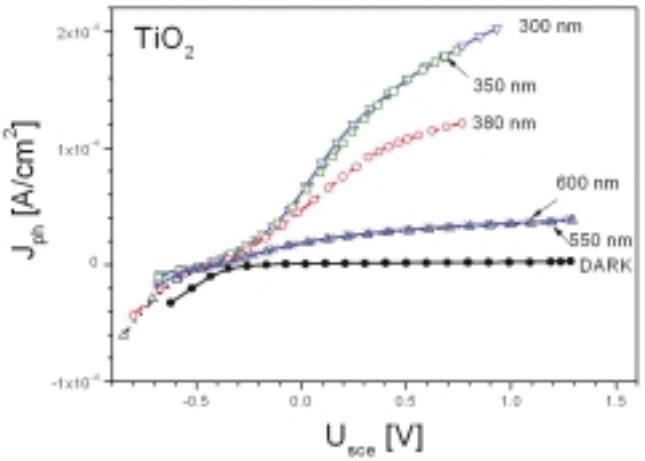

Figure 7. Current-voltage characteristics for undoped TiO_2 monitored in dark and after illumination by monochromatic light.

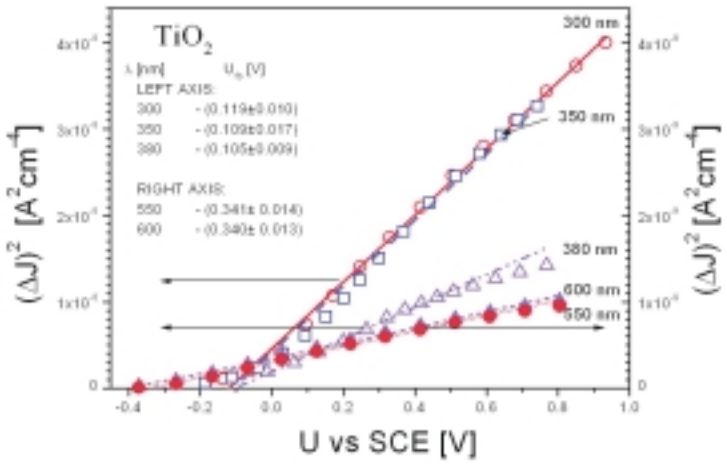

Figure 8. The square of the anodic current induced by monochromatic light as a function of the electrode potential (*vs* SCE) for undoped TiO_2; left axis: λ = 300 nm, 350 nm and 380 nm; right axis: λ = 550 nm and 600 nm.

Much slower changes of photocurrent with time are observed for W-doped materials than that for undoped TiO_2. Examples of such kinetics are illustrated in Figs 9 and 10 for concentration of tungsten 0.1 at % and 0.2 at %, respectively. Time required to achieve a new value of current after either light on or light off is about 10–15 s for undoped TiO_2 (see Figs 2 and 3). On the other hand, this time is above 500 s for TiO_2 + 0.1 at % W (Fig. 9) and for TiO_2 + 0.2 at % W (Fig.10).

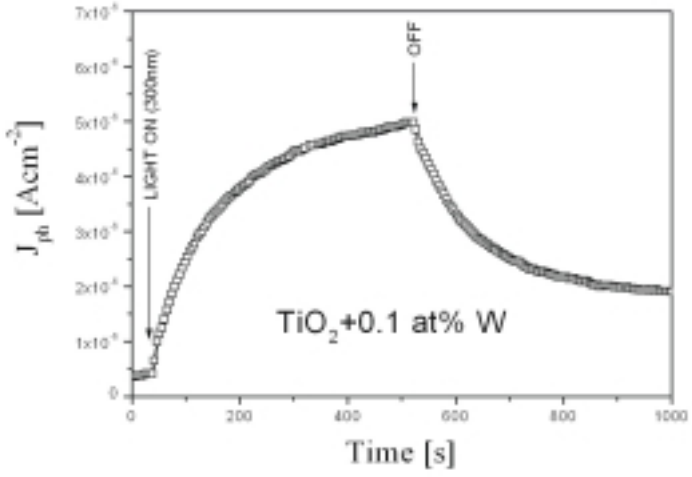

Figure 9. Kinetics of photocurrent of TiO_2 + 0.1 at % W, induced by monochromatic light of 300 nm.

The presented above photocurrent studies, using monochromatic and white light, allow us to determine 2 efficiencies of a PEC, incident photon-to-current efficiency IPCE and sollar-to-hydrogen conversion efficiency STH, respectively. IPCE is defin-

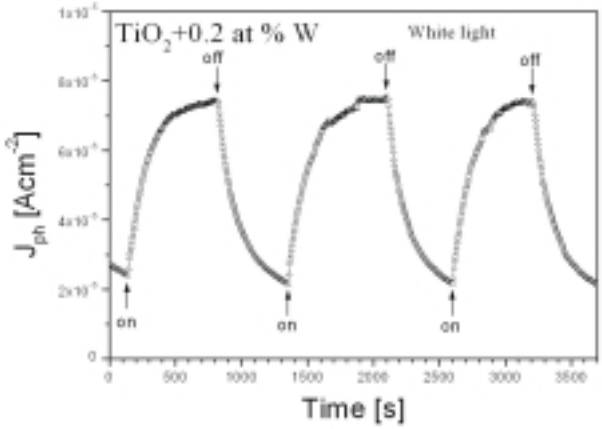

Figure 10. Kinetics of photocurrent of TiO_2 + 0.2 at % W, induced by white light.

ed by the number of electrons generated by light in the external circuit divided by the number of incident photons [29]:

$$IPCE = \frac{hcJ_\lambda}{\lambda W_\lambda} \tag{5}$$

where: h – Planck's constant, c – velocity of light, J_λ – photocurrent density, λ – wavelength, W_λ – power of monochromatic light flux. Stating J_λ in A/cm^2, λ in nm and W_λ in W/m^{-2} , the relationship (5) assumes the following form:

$$IPCE = \frac{1240J_\lambda}{\lambda W_\lambda} \tag{6}$$

Fig. 11 shows IPCE as a function of wavelength for undoped TiO_2 and TiO_2 + 0.2 at % W. Two regions of wavelength can be distinguished. IPCE determined for photons with energy lower than energy gap E_g in TiO_2 assumes values below 1.25% for both undoped and tungsten-doped material. On the other hand, the abrupt changes of IPCE with wavelength is observed for photons with energy $E_{photon} > E_g$. IPCE tungsten-doped TiO_2 assumes slightly lower values than that of undoped electrode.

Solar-to-hydrogen conversion efficiency STH can be determined from the relation [30]:

$$STH = \frac{I(1.23 - U_{bias})}{WS} \tag{7}$$

where W is the power of incidence solar irradiation, S – surface of irradiated electrode. Fig. 12 shows STH parameter as a function of bias voltage. Strong effect of tungsten doping on STH parameter is observed. Sample containing 0.1 at % W exhib-

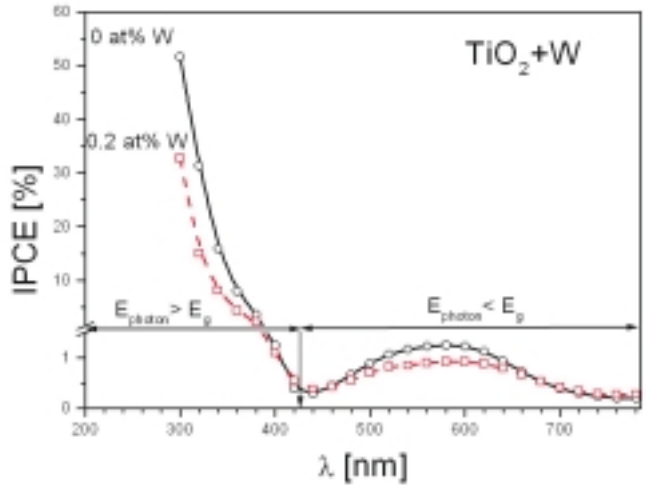

Figure 11. Incident photon-to-current efficiency, IPCE *vs* wavelength.

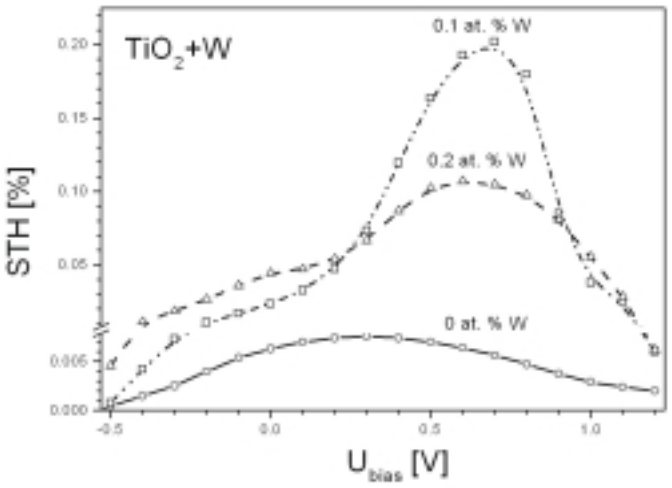

Figure 12. Solar-to-hydrogen energy conversion efficiency, SHE *vs* electrical bias.

its the highest efficiency. The optimal electrical bias is *ca* 0.3 V for undoped and *ca* 0.6–0.7 V for tungsten-doped material.

Conclusions

Undoped and W-doped TiO_2 polycrystalline specimens used as photoelectrodes for water decomposition were the subject of investigations. The transient time constant of undoped electrode is about 31.6 s for white light. Time needed to achieve steady-state after either light on or light off is about 10–15 s for undoped material. This time is *ca* 40 times longer for W-doped specimens. The determined flat band potential of TiO_2 at pH = 7.8 is: $U_{fb} = -(0.11 \pm 0.01)$ V in respect to the saturated calomel electrode.

Quantum efficiency expressed by incident photon-to-current efficiency, IPCE strongly increases with photon energy (for $E_{photon} > E_g$) achieving 52% and 32% at wavelength $\lambda = 300$ nm for undoped and doped with 0.2 at % W, respectively. Doping of TiO_2 with tungsten enhances solar-to-hydrogen conversion energy efficiency, STH. TiO_2 containing 0.1 at % W exhibits highest STH. The maximum energy conversion efficiency has been observed for voltage bias *ca* 0.3 V for undoped and *ca* 0.65 V for tungsten-doped TiO_2.

Acknowledgments

This work was supported by the Polish State Committee for Scientific Research (KBN) in the grant 11.11.160.247.

REFERENCES

1. Fujishima A. and Honda K., *Nature*, **238**, 37 (1972).
2. Ghosh A.K. and Maruska H.P., *J. Electrochem. Soc*., **124**, 1516 (1977).
3. Julião J.F., Decker F. and Abramovich R.M., *J. Electrochem. Soc.,* **127**, 2264 (1980).
4. Akikusa J. and Khan S.U.M., *Int. J. Hydrogen Energy,* **22**, 875 (1997).
5. Gautron J., Lemasson P. and Marucco J.F., *Faraday Disc*., **70**, 81 (1980).
6. Kogan Ya.L. and Vakulenko A.M., *Solar Energy Mater.*, **3**, 357 (1980).
7. Matsumoto Y., Kurimoto J., Amagasaki Y. and Sato E., *J. Electrochem. Soc.,* **127**, 2148 (1980).
8. Bak T., Nowotny J., Rekas M. and Sorell C.C., *Int. J. Hydrogen Energy,* **27**, 19 (2002).
9. Matsumoto Y., Kurimoto J., Schimizu T. and Sato E*., J. Electrochem. Soc*., **128**, 1040 (1981).
10. Monnier A. and Augustynski J., *J. Electrochem. Soc*., **127**, 1576 (1980).
11. Giordano N., Antonucci V., Cavallaro S., Lembo R. and Bart J.C.J*., Int. J. Hydrogen Energy*, **7**, 867 (1982).
12. Di Quatro F., Piazza S. and Sunseri C., *Electrochim. Acta,* **38**, 29 (1993).
13. Radecka M., Wierzbicka M. and Rekas M., *Physica C*, in print.
14. Bak T., Nowotny J., Rekas M. and Sorrell C.C*., Int. J. Hydrogen Energy,* **27**, 991 (2002).
15. Grant F.A., *Rev. Modern Phys.*, **31**, 647 (1959).
16. Salvador P., *Solar Energy Mater.*, **2**, 413 (1980).
17. Madou M.J., Kinoshita K. and McKubre M.C.H., *Electrochim. Acta*, **29**, 419 (1984).
18. Wrighton M.S., Ellis A.B., Wolczanski P.T., Morse D.L., Abrahamson H.B. and Ginley D.S., *J. Am. Chem. Soc*., **98**, 2774 (1976).
19. Gennari F.C. and Pasquievich D.M., *J. Am. Ceram. Soc*., **82**, 1915 (1999).
20. Gajerski R., Radecka M., Wierzbicka M. and Rekas M., *J. Therm. Anal. Calorim*., **76**, 949 (2004).
21. Radecka M., Wierzbicka M., Komornicki S. and Rekas M., *Physica B*, **348**, 160 (2004).
22. Tafalla D., Salvador P. and Benito R.M., *J. Electrochem. Soc*., **137**, 1810 (1990).
23. Hagfeldt A., Lindström H., Södergren S. and Lindquist S.E*., J. Electroanal. Chem*., **381**, 39 (1995).
24. CRC Handbook of Chemistry and Physics, CRC Press Inc., 60-th edition p. D156.
25. Bak T., Nowotny J., Rekas M. and Sorrell C.C., *J. Phys. Chem. Solid*, **64**, 1043 (2003).
26. Butler M.A., Abramovich A., Decker F. and Juliao J.F*., J. Electrochem. Soc*., **122**, 200 (1981).
27. Finklea H.O., Semiconductor electrodes, Finklea H.O, Ed., Elsevier Sci. Publ., NY 1988, pp. 115–119.
28. Pleskov Yu.V. and Gurevich Yu.Ya., Semiconductor Photoelectrochemistry, Bartlett P.N. (Translation Ed.). Consultants Bureau NY, London 1986, pp. 179–208.
29. Gerischer J., Solar energy conversion, Seraphin B.O., Ed., Springer, Berlin, 1979 pp. 115–172.
30. Parkinson B., *Acc. Chem. Res*., **17**, 431 (1984).